OPTICAL IDENTIFICATION OF MULTIPLE FAINT X-RAY SOURCES IN THE GLOBULAR CLUSTER NGC 6752: EVIDENCE FOR NUMEROUS CATACLYSMIC VARIABLES[1]

DAVID POOLEY,[2] WALTER H. G. LEWIN,[2] LEE HOMER,[3] FRANK VERBUNT,[4] SCOTT F. ANDERSON,[3] BRYAN M. GAENSLER,[2,5,6] BRUCE MARGON,[7] JON M. MILLER,[2] DEREK W. FOX,[8] VICTORIA M. KASPI,[2,9] AND MICHIEL VAN DER KLIS[10]

ABSTRACT

We report on the *Chandra X-Ray Observatory* ACIS-S3 imaging observation of the globular cluster NGC 6752. We detect six X-ray sources within the $10''.5$ core radius and 13 more within the $115''$ half-mass radius down to a limiting luminosity of $L_X \approx 10^{30}$ ergs s^{-1} for cluster sources. We reanalyze archival data from the *Hubble Space Telescope* and the Australia Telescope Compact Array and make 12 optical identifications and one radio identification. Based on X-ray and optical properties of the identifications, we find 10 likely cataclysmic variables (CVs), one to three likely RS CVn or BY Dra systems, and one or two possible background objects. Of the seven sources for which no optical identifications were made, we expect that approximately two to four are background objects and that the rest are either CVs or some or all of the five millisecond pulsars whose radio positions are not yet accurately known. These and other *Chandra* results on globular clusters indicate that the dozens of CVs per cluster expected by theoretical arguments are being found. The findings to date also suggest that the ratio of CVs to other types of X-ray sources is remarkably similar in clusters of very different structural parameters.

Subject headings: binaries: close — globular clusters: general — globular clusters: individual (NGC 6752) — novae, cataclysmic variables — X-rays: stars

1. INTRODUCTION

Globular clusters are very efficient catalysts in forming unusual objects, such as low-mass X-ray binaries (LMXBs), cataclysmic variables (CVs), millisecond pulsars (MSPs), and blue stragglers, with formation rates per unit mass exceeding those in the Galactic disk by orders of magnitude. The high stellar densities in globular clusters trigger various dynamical interactions: exchanges in encounters with binaries, direct collisions, destruction of binaries, and perhaps tidal capture. Many details of these processes are not well understood, primarily because of the complex feedback between stellar evolution and stellar dynamics. The rate of these competing processes depends strongly on the cluster's physical properties. For example, binary formation by tidal capture generally requires higher densities than do exchange reactions involving primordial binaries (Hut et al. 1992). In the outermost regions of even the densest clusters, the currently observed binaries will be mainly primordial ones. In contrast, the LMXBs and MSPs that consequently evolve from the LMXBs are formed (almost) exclusively via stellar encounters. Davies & Hansen (1998) have shown how the large number of binary radio pulsars that are present in 47 Tuc (Camilo et al. 2000; Freire et al. 2001) may have been formed from an initial population of some 10^6 primordial binaries and $\sim 10^4$ neutron stars.

To date, there are 13 known bright ($L_X \gtrsim 10^{36}$ ergs s^{-1}) X-ray sources in 12 globular clusters. The X-ray spectra and luminosities indicate that these are LMXBs; orbital periods from 11 minutes to 17.1 hr have been determined for five sources. In 11 sources, type I X-ray bursts have been detected (in 't Zand et al. 1999 and references therein), which are well explained as thermonuclear runaways on a neutron star surface (for a review, see Lewin, van Paradijs, & Taam 1993). Optical counterparts have been found for six bright sources (Deutsch et al. 1998; Heinke, Edmonds, & Grindlay 2001; Homer et al. 2001 and references therein).

With the *Einstein* satellite, seven faint ($L_X \lesssim 10^{35}$ ergs s^{-1}) sources were detected in the cores of as many clusters (Hertz & Grindlay 1983a, 1983b). With *ROSAT*, the number of faint core sources (within two core radii of the centers) expanded to 40, including multiple sources in 47 Tuc, ω Cen, NGC 6397, NGC 6752, and others; an additional 17 faint sources were found farther out in the clusters (more than 2 core radii from the centers). Whereas virtually all of the core sources are related to the globular clusters, some of the sources outside the cores may be in the background or foreground (Verbunt 2001 and references therein). Because of crowding and the limited accuracy of even the *ROSAT* positions (varying from $2''$ to $5''$, depending on whether a

[1] Based on observations with the NASA/ESA *Hubble Space Telescope*, obtained at the Space Telescope Science Institute, which is operated by AURA, Inc., under NASA contract NAS 5-26555.

[2] Center for Space Research and Department of Physics, Massachusetts Institute of Technology, 70 Vassar Street, Building 37, Cambridge, MA 02139-4307; davep@space.mit.edu, lewin@space.mit.edu, jmm@space.mit.edu.

[3] Department of Astronomy, Box 351580, University of Washington, Physics/Astronomy Building, Stevens Way, Box 351580, Seattle, WA 98195; homer@astro.washington.edu, anderson@astro.washington.edu.

[4] Astronomical Institute, Utrecht University, P.O. Box 80000, 3508 TA Utrecht, Netherlands; f.w.m.verbunt@astro.uu.nl.

[5] Current address: Harvard-Smithsonian Center for Astrophysics, 60 Garden Street, Cambridge, MA 02138; bgaensler@cfa.harvard.edu.

[6] Hubble Fellow.

[7] Space Telescope Science Institute, 3700 San Martin Drive, Baltimore, MD 21218; margon@stsci.edu.

[8] Department of Astronomy, California Institute of Technology, Mail Code 105-24, Pasadena, CA 91125; derekfox@astro.caltech.edu.

[9] Department of Physics, Rutherford Physics Building, McGill University, 3600 University Street, Montreal, QC H3A 2T8, Canada; vkaspi@physics.mcgill.ca.

[10] Astronomical Institute "Anton Pannekoek," University of Amsterdam and Center for High-Energy Astrophysics, Kruislaan 403, 1098 SJ Amsterdam, Netherlands; michiel@astro.uva.nl.

secure optical identification allows accurate determination of the bore sight correction), optical identifications of faint X-ray sources in globular cluster cores remained tentative before the *Chandra* era, and some suggestions have been disproved with more accurate X-ray positions, as in 47 Tuc (Verbunt & Hasinger 1998) and M92 (Geffert 1998; Verbunt 2001). The only secure optical identification was that of a dwarf nova with a faint X-ray source 12 core radii from the center of NGC 5904 (Hakala et al. 1997; Margon, Downes, & Gunn 1981). The radio pulsar in M28 is another securely identified faint X-ray source (Lyne et al. 1987; Saito et al. 1997). Some identifications, like those in M13, remain in doubt (Verbunt 2001).

Progress in identifying the nature of the various faint X-ray sources has been very slow during the past two decades. However, this is now rapidly changing. With *Chandra*'s high sensitivity and unprecedented spatial resolution of $\sim 1''$, a revolution is underway in our understanding of the low-luminosity globular cluster X-ray sources and their association with the binary populations of globular clusters. To date, some results have already been reported for a 74 ks observation of 47 Tuc (Grindlay et al. 2001a), a 70 ks observation of ω Cen (Rutledge et al. 2001a), and a 49 ks observation of NGC 6397 (Grindlay et al. 2001b), and preliminary results have been reported for our own observations of NGC 6752, NGC 6440, and NGC 6121 (Pooley et al. 2000). The *Chandra* observations have confirmed previously suggested optical counterparts for faint X-ray sources in the cores of these clusters and made numerous additional identifications. We report here in more detail on the results of a 30 ks observation of NGC 6752. In § 6 we will compare our results with those reported earlier.

NGC 6752 is at a distance of 4.1 ± 0.2 kpc (Renzini et al. 1996). The optically derived center is at (J2000.0) $19^h 10^m 51 \overset{s}{.} 8$, $-59°58'55''$ (Harris 1996). Its moderate optical reddening $E_{B-V} = 0.04$ may be converted to a nominal X-ray absorption column characterized by $N_H = 2.2 \times 10^{20}$ cm^{-2} using the relation found by Predehl & Schmitt (1995). Its core radius r_c is $10\overset{''}{.}5$, and its half-mass radius r_h is $115''$ (Trager, Djorgovski, & King 1993). We use these values throughout the paper.

Faint X-ray sources in NGC 6752 were first found by Grindlay (1993) on the basis of a 31.3 ks *ROSAT* HRI exposure, which revealed a double source in the core and two sources outside the core but within the half-mass radius. These sources were also detected with the *ROSAT* PSPC (Johnston, Verbunt, & Hasinger 1994). Verbunt & Johnston (2000) co-added three *ROSAT* HRI observations for a total exposure of 72 ks and identified an X-ray source with the noncluster member star Tyc 9071 228 1, allowing an accurate solution of the bore sight correction and therewith an accurate ($\sigma \simeq 2''$) absolute positioning of the X-ray frame. They also resolved the central source into four sources and argued on the basis of the source density in the whole *ROSAT* image that the other sources within the half-mass radius were possibly related to the cluster. The best position for the northernmost *ROSAT* source in the core is marginally compatible with the previously published position of the southern of two Hα emission objects and photometric variables with periods of 5.1 and 3.7 hr discovered with *Hubble Space Telescope* (*HST*) observations by Bailyn et al. (1996).

Our *Chandra* X-ray observations are described and analyzed in § 2, our radio observations in § 3, and our analysis

of the *HST* observations in § 4. The results are described in § 5 and discussed in § 6.

2. X-RAY OBSERVATIONS

NGC 6752 was observed with the *Chandra X-Ray Observatory* (Weisskopf, O'Dell, & van Speybroeck 1996) for ~ 30 ks on 2000 May 15. The observation was made with the Advanced CCD Imaging Spectrometer (ACIS) with the telescope aim point on the back side–illuminated S3 chip, which offers increased sensitivity to low-energy X-rays compared to the front side–illuminated chips. The entire region inside the cluster's half-mass radius fit on the 8.3 arcmin^2 S3 chip. The data were taken in timed exposure mode with the standard integration time of 3.24 s per frame and telemetered to the ground in faint mode, in which a 3×3 pixel island is recorded for each event.

2.1. *X-Ray Data Reduction*

Data reduction was performed using the CIAO 2.1 software provided by the *Chandra* X-Ray Center.[11] We used the CALDB, Version 2.6, calibration files (gain maps, quantum efficiency, quantum efficiency uniformity, effective area). Bad pixels were excluded, as were intervals of background flaring (~ 1 ks). The effective exposure time for the observation after filtering for flares and correcting for dead time was 28.7 ks.

Starting with the raw (level 1) event list, we processed the data (using "acis_process_events") without including the pixel randomization that is added during standard processing.[12] This method slightly improves the point spread function (PSF). We then applied good-time intervals (both the ones supplied with the standard data products and our custom ones, which excluded the period of background flaring) and filtered the data to include only events with *ASCA* grades of 0, 2, 3, 4, or 6 (this is the "standard" choice that generally optimizes the signal-to-background ratio; see the *Chandra* Proposer's Observatory Guide available from the *Chandra* X-Ray Center Web site[13] for more information). We also excluded software-flagged cosmic-ray events. We used this filtered event list (level 2) for the subsequent analysis.

2.2. *X-Ray Source Detection*

The wavelet-based "wavdetect" tool was employed for source detection. We found that the detection of sources was insensitive to whether we used a medium-band (0.5–4.5 keV) or full-band (0.3–8.0 keV) image. We detected 19 point sources within the cluster half-mass radius (Table 1) and another 21 on the rest of the S3 chip. We have numbered the sources in order of most to least counts in the 0.5–6.0 keV band. Our detection threshold was ≥ 5 counts in the 0.3–8.0 keV image. The absorbed flux of the faintest detected source was $\sim 6 \times 10^{-16}$ ergs cm^{-2} s^{-1}. Using the density of sources outside the half-mass radius, we estimate that about four sources within the half-mass radius are not

---

[11] See http://asc.harvard.edu.

[12] This randomization has the effect of removing the artificial substructure (Moiré pattern) that results as a byproduct of spacecraft dither. Since all of our observations contained a substantial number of dither cycles (one dither cycle has a period of ~ 1000 s), this substructure is effectively washed out, and there is no need to blur the image with pixel randomization.

[13] See footnote 11.

TABLE 1
NGC 6752 X-Ray Sources

Source[a]	R.A. (J2000.0)[b]	Decl. (J2000)[b]	Detected Counts/Corrected Counts[c]			L_X (0.5–2.5 keV) (ergs s^{-1})[d]	Counterpart[e]	ID[f]
			X_{soft}	X_{med}	X_{hard}			
CX 1	19 10 51.098	−59 59 11.83	536/588.0	936/1014.0	444/457.0	2.1×10^{32}	Opt./X7b	CV
CX 2	19 10 55.972	−59 59 37.33	196/215.3	315/343.5	130/135.3	6.0×10^{31}	Opt./X14	CV
CX 3	19 10 40.318	−59 58 41.29	177/195.4	274/297.6	104/107.0	5.3×10^{31}	Opt./X6	CV
CX 4	19 10 51.546	−59 59 01.71	132/146.0	219/238.7	94/97.1	4.0×10^{31}	Opt./B1	CV
CX 5	19 10 51.374	−59 59 05.11	94/103.7	175/190.3	86/88.7	3.6×10^{31}	Opt.	CV/BY Dra
CX 6	19 10 51.462	−59 59 26.99	83/90.9	121/130.9	41/42.1	2.2×10^{31}	Opt./X22	CV
CX 7	19 10 51.467	−59 58 56.72	58/64.3	95/103.6	44/45.4	1.9×10^{31}	Opt./B2	CV
CX 8	19 11 02.944	−59 59 41.89	83/90.8	87/94.5	4/3.9	2.1×10^{31}	...	
CX 9	19 10 51.720	−59 58 59.16	47/52.0	65/70.8	19/19.5	1.3×10^{31}	...	
CX 10......	19 10 54.706	−59 59 13.87	13/14.2	25/27.0	12/12.3	6.0×10^{30}	Opt.	CV
CX 11......	19 10 52.376	−59 59 05.56	22/24.1	26/28.0	5/5.0	6.2×10^{30}	Opt.	CV/Gal.
CX 12......	19 10 52.694	−59 59 03.27	19/20.8	23/24.7	4/3.9	5.6×10^{30}	...	
CX 13......	19 10 40.565	−60 00 06.07	13/13.8	18/18.6	7/6.8	4.6×10^{30}	Opt.	CV
CX 14......	19 10 52.039	−59 59 09.12	15/16.4	15/16.0	0/−	4.2×10^{30}	...	
CX 15......	19 10 55.798	−59 57 45.53	8/8.5	10/10.4	2/1.9	3.2×10^{30}	Opt.	CV/Gal.
CX 16......	19 10 42.474	−59 58 42.83	8/8.7	9/9.5	1/0.9	3.0×10^{30}	Opt.	BY Dra
CX 17......	19 11 05.279	−59 59 04.03	3/3.2	7/7.4	4/4.0	2.7×10^{30}	Rad.	MSP/Gal.
CX 18......	19 10 52.006	−59 59 03.69	7/7.7	7/7.5	0/−	2.7×10^{30}	...	
CX 19......	19 10 55.577	−59 59 17.54	4/4.3	4/4.2	0/−	2.2×10^{30}	...	

Note.—Units of right ascension are hours, minutes, and seconds, and units of declination are degrees, arcminutes, and arcseconds.

[a] Sources are numbered according to their total counts.

[b] The *Chandra* positions have been corrected by $-0\overset{s}{.}044$ ($=-0\overset{''}{.}33$) in right ascension and $-0\overset{''}{.}17$ in declination (see § 3). We estimate the uncertainties in the final astrometric solution at about $0\overset{''}{.}3$ in both right ascension and declination. These uncertainties are much larger than the "wavdetect" centroiding uncertainties.

[c] Corrections are described in § 2.3. X-ray bands are 0.5–1.5 keV (X_{soft}), 0.5–4.5 keV (X_{med}), and 1.5–6.0 keV (X_{hard}).

[d] For sources CX 1–CX 9, L_X comes from an average of the unabsorbed luminosities of the best-fit models for each source (see Tables 2 and 3). A linear relation between L_X and X_{med} counts for these sources was derived and used to estimate L_X for sources CX 10–CX 19 based on their X_{med} counts. Typical uncertainties in L_X are ~20%.

[e] Type of counterpart (optical or radio) found and associations (if any) with previously reported sources. The "X" numbers refer to the *ROSAT* sources of Verbunt & Johnston 2000. The "B" numbers refer to the *HST* sources of Bailyn et al. 1996. Note that our *HST* positions for these variables are very different from those given by Bailyn et al. (see § 4.1).

[f] See § 5 for details. "Gal." indicates that the source may be a galaxy.

associated with the cluster, which is in approximate agreement with the $\log N$–$\log S$ relationships of Giacconi et al. (2001). All 19 possible cluster sources are consistent with being point sources, with the possible exception of CX 12. Comparing the observed radial surface brightness profile of this source to one predicted for a source of its intensity and at its location on the chip, we find that it is inconsistent with being a single point source at 94% confidence ($\chi^2 = 12.2$ for 6 degrees of freedom [dof]). It is most likely a blend of multiple sources.

The central $1\overset{'}{.}6$ portion of NGC 6752 is shown in Figure 1. Overlaid on this image are the source extraction regions determined by "wavdetect," with a dashed circle indicating the core radius and a cross indicating the optical center of the cluster.

2.3. *X-Ray Count Rates*

Source counts were extracted in a variety of energy bands. We found that the most useful data were between 0.5 and 6.0 keV since this range preserved almost all of the source counts while limiting the background contribution. We focus on the following bands for hardness ratios and the X-ray color-magnitude diagram (CMD): 0.5–1.5 keV (X_{soft}), 0.5–4.5 keV (X_{med}), and 1.5–6.0 keV (X_{hard}). While somewhat arbitrary, this choice allows a direct comparison with the results of Grindlay et al. (2001a) on 47 Tuc, which has a similar distance and column density.

The detected count rate was corrected for background, exposure variations, and foreground photoelectric absorption. The background count rate in each band was estimated from an annulus around the innermost sources. The inner radius was 29″, and the outer radius was 70″. No sources were present within the annulus. Because of the spacecraft's dither, some sources passed in and out of bad columns on the CCD. To account for the ~4% variations in exposure that resulted, we applied multiplicative corrections based on the ratio of a source's average effective area in each of the three bands to the average effective area in the same band of CX 15, which had the highest average exposure. The individual effective area curves for the sources were made using the CIAO tool "mkarf." The average effective area of CX 15 in each of the bands was 591 (X_{soft}), 465 (X_{med}), and 377 cm^2 (X_{hard}).

To correct for the column density to NGC 6752, we used XSPEC (Arnaud 1996) to examine the effects of absorption on three spectra characteristic of what one might expect to find in a globular cluster: a 3 keV thermal bremsstrahlung (for CVs; Richman 1996; van Teeseling, Beuermann, & Verbunt 1996), a 0.3 keV blackbody (for quiescent LMXBs; Verbunt et al. 1994; Asai et al. 1996, 1998; as a substitute for the more correct neutron star atmosphere models, see Rutledge et al. 2001b and references therein), and a power law with a photon index of $\Gamma = 2$ (for MSPs; Becker & Trümper 1999). In each of our three bands, we took the ratio of the
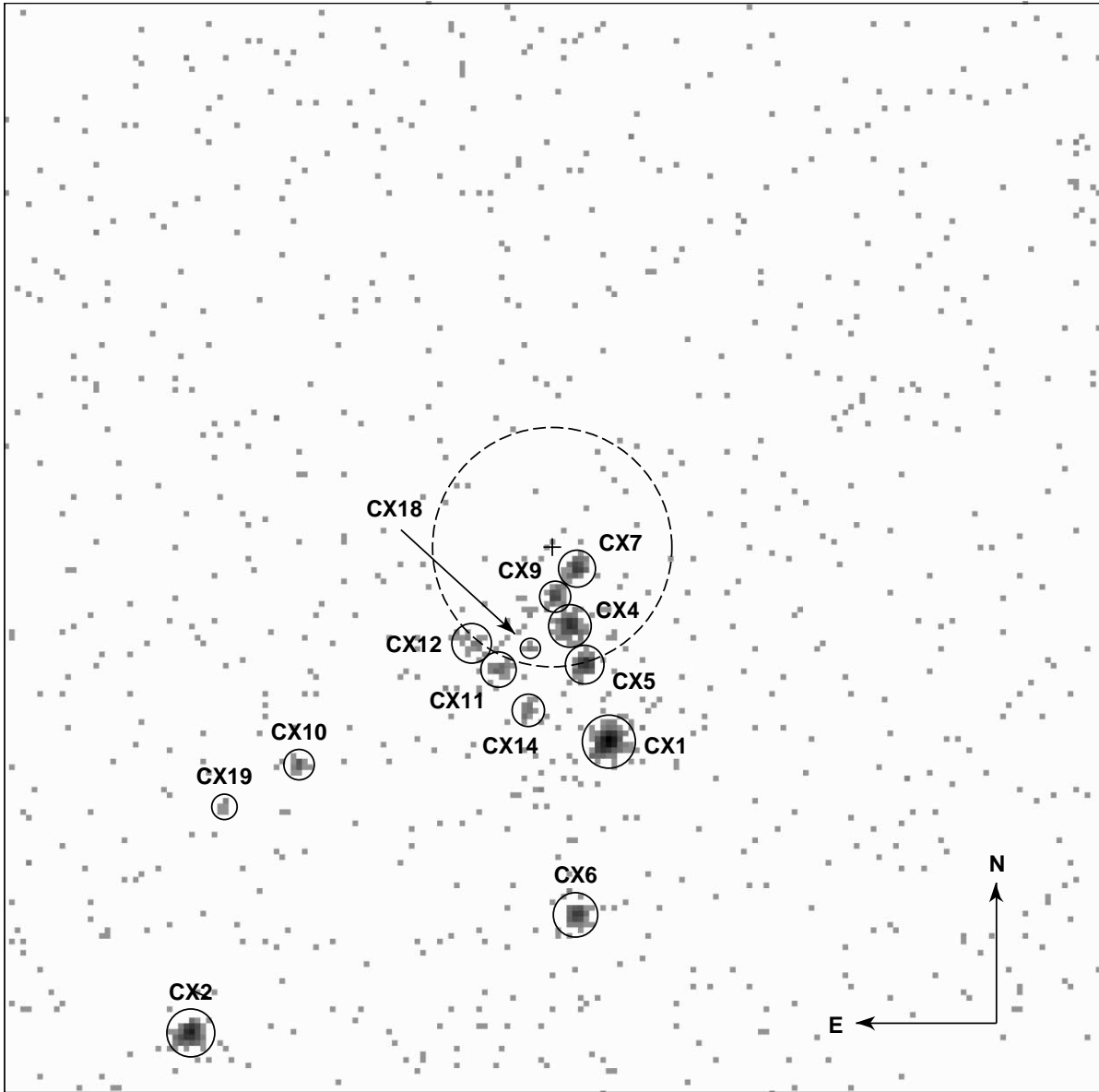
Fɪɢ. 1.—X-ray image of the central $1'.6 \times 1'.6$ region of NGC 6752. The solid circles indicate the source extraction regions as determined by "wavdetect." The optical cluster center is indicated with a cross, and the dashed circle is the $10''.5$ core radius of the cluster. Each pixel is a $0''.492$ square.

unabsorbed count rate to one absorbed by a column density of $N_H = 2.2 \times 10^{20}$ cm^{-2}. Because this is a fairly low column density, the effects were small on each of the three model spectra. We used a simple average of the ratios to derive the following correction factors for the observed count rate in each band: 1.084 (X$_{soft}$), 1.067 (X$_{med}$), and 1.010 (X$_{hard}$). Table 1 lists both the observed and fully corrected counts in each band for all 19 sources. The X-ray CMD based on the corrected counts is shown in Figure 2. Note that the effect on the X-ray CMD of the correction for absorption is a uniform shift of all points 0.03 units up and 0.02 units to the right.

2.4. X-Ray Spectral Fitting

We used the CIAO tool "dmextract" to extract spectra of the brighter sources (CX 1–CX 9) and "dmgroup" to group the spectra to a selected number of counts per bin.

CX 1 was grouped to contain $\geq$35 counts bin^{-1}, CX 2–CX 4 were grouped at $\geq$15 counts bin^{-1}, and CX 5–CX 9 at $\geq$10 counts bin^{-1}. Background-subtracted spectral modeling was performed with XSPEC using data in the 0.3–8.0 keV range.

We fitted three different models to each of the nine brightest sources (CX 1–CX 9): thermal bremsstrahlung, blackbody, and power law. For CX 1, the column density was allowed to vary and was compared to a fixed value of $N_H = 2.2 \times 10^{20}$ cm^{-2} for the cluster. For the other sources, however, we found that the data could not constrain N_H well and that all best-fit values were consistent with the column density from optical reddening. We therefore fixed N_H at the optical reddening value for the rest of the sources. The results are listed in Tables 2 and 3.

From the best-fit models, we calculated the unabsorbed source luminosities for CX 1–CX 9. Averaging the results from the best fits of each of the three models, we arrived at
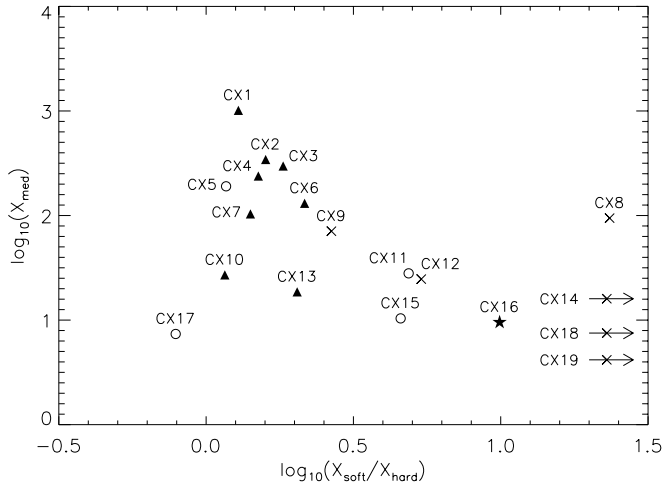
Fig. 2.—X-ray CMD for NGC 6752. The X-ray color is defined as the logarithm of the ratio of X_{soft} (0.5–1.5 keV) corrected counts to X_{hard} (1.5–6.0 keV) corrected counts, and the magnitude is the logarithm of X_{med} (0.5–4.5 keV) corrected counts. Probable source natures are indicated by symbols (*filled triangles*: CVs; *star*: BY Dra; *circles*: ambiguous sources with optical or radio counterparts; *crosses*: sources with no radio or optical counterparts). The arrows indicate the magnitudes of the three sources (CX 14, CX 18, and CX 19) for which there were no detected counts in X_{hard}.

our estimate for the source luminosities listed in Table 1. The major sources of uncertainty in these luminosities arise from the scatter in the luminosities from the three different models and the uncertainties in each individual fit. The com-

TABLE 2
Spectral Fits to the *Chandra* Data of the Brighter Sources for fixed $N_H = 2.2 \times 10^{20}$ cm^{-2}

Source	Model[a]	kT (keV)	L_X (0.5–2.5 keV) (ergs s^{-1})[b]	χ^2_{red} (dof)
CX 1	TB	$99.8^{+\infty}_{-66.4}$	1.8×10^{32}	1.04 (25)
	BB	$0.66^{+0.05}_{-0.04}$	2.0×10^{32}	4.05 (25)
	PL	$1.19^{+0.07}_{-0.09}$	1.7×10^{32}	1.17 (25)
CX 2	TB	$20.8^{+146}_{-72.4}$	6.0×10^{31}	1.02 (19)
	BB	$0.45^{+0.08}_{-0.07}$	6.0×10^{31}	3.48 (19)
	PL	$1.32^{+0.15}_{-0.13}$	5.9×10^{31}	1.03 (19)
CX 3	TB	$5.20^{+4.6}_{-1.9}$	5.3×10^{31}	1.20 (16)
	BB	$0.50^{+0.08}_{-0.11}$	5.5×10^{31}	3.53 (16)
	PL	$1.62^{+0.17}_{-0.17}$	5.2×10^{31}	1.23 (16)
CX 4	TB	$17.1^{+117}_{-10.2}$	4.2×10^{31}	1.05 (12)
	BB	$0.61^{+0.10}_{-0.10}$	3.6×10^{31}	2.90 (12)
	PL	$1.35^{+0.18}_{-0.17}$	4.1×10^{31}	1.14 (12)
CX 5	TB	> 29	3.5×10^{31}	0.84 (14)
	BB	$0.65^{+0.12}_{-0.11}$	3.6×10^{31}	1.07 (14)
	PL	$0.93^{+0.25}_{-0.25}$	3.5×10^{31}	0.66 (14)
CX 6	TB	$11.7^{+126}_{-7.2}$	2.2×10^{31}	1.02 (10)
	BB	$0.38^{+0.11}_{-0.07}$	2.2×10^{31}	2.41 (10)
	PL	$1.41^{+0.24}_{-0.22}$	2.2×10^{31}	1.06 (10)
CX 7	TB	$34.2^{+\infty}_{-29.1}$	2.0×10^{31}	0.78 (8)
	BB	$0.45^{+0.31}_{-0.13}$	1.8×10^{31}	3.12 (8)
	PL	$1.33^{+0.35}_{-0.35}$	1.9×10^{31}	0.71 (8)
CX 8	TB	$6.32^{+\infty}_{-5.0}$	2.2×10^{31}	2.07 (6)
	BB	$0.26^{+0.05}_{-0.04}$	1.7×10^{31}	1.35 (6)
	PL	$1.31^{+0.48}_{-0.49}$	2.3×10^{31}	2.11 (6)
CX 9	TB	$3.34^{+115}_{-2.0}$	1.3×10^{31}	0.14 (4)
	BB	$0.34^{+0.10}_{-0.07}$	1.3×10^{31}	0.49 (4)
	PL	$1.64^{+0.48}_{-0.47}$	1.3×10^{31}	0.21 (4)

[a] TB: thermal bremsstrahlung; BB: blackbody; PL: power law.
[b] Unabsorbed luminosity for $d = 4.1$ kpc.

TABLE 3
Spectral fits to the *Chandra* Data of CX 1 with N_H Allowed to Vary

Model[a]	N_H ($\times 10^{20}$ cm^{-2})	kT (keV)	L_X (0.5–2.5 keV) (ergs s^{-1})[b]	χ^2_{red} (dof)
TB..............	$8.36^{+1.61}_{-3.21}$	$15.9^{+21.0}_{-6.3}$	2.1×10^{32}	0.66 (24)
BB..............	< 0.48	$0.67^{+0.04}_{-0.04}$	1.9×10^{32}	3.70 (24)
PL..............	$10.4^{+4.0}_{-3.7}$	$1.44^{+0.14}_{-0.13}$	2.2×10^{32}	0.73 (24)
BB + PL	$1.99^{+10.9}_{-1.99}$	$kT = 0.67^{+0.32}_{-0.17}$ ($\Gamma = 1.23^{+0.36}_{-0.15}$)	1.9×10^{32}	0.54 (22)

[a] TB: thermal bremsstrahlung; BB: blackbody; PL: power law.
[b] Unabsorbed luminosity for $d = 4.1$ kpc.

bined effect is typically around 20%. The uncertainties in distance (2.4%) and column density (1.7%) are negligible in comparison.

Fitting a linear relation to the CX 1–CX 9 luminosities versus the corrected counts in X_{med}, we have estimated the unabsorbed luminosities for sources CX 10–CX 19 based on their X_{med} counts. These are also listed in Table 1.

3. RADIO OBSERVATIONS

We have analyzed archival radio observations of NGC 6752, carried out on 1995 February 2 using the Australia Telescope Compact Array (ATCA; Frater, Brooks, & Whiteoak 1992). Observations were made simultaneously at 1.4 and 2.4 GHz and cover the entire *Chandra* field of view. At 1.4 and 2.4 GHz, the resulting spatial resolutions are $5''.7 \times 4''.9$ and $3''.2 \times 2''.7$ with sensitivities of 70 and 90 μJy beam^{-1}, respectively (where 1 Jy = 10^{-26} W m^{-2} Hz^{-1}).

We find three source coincidences between the X-ray and 1.4 GHz radio images: one point source within the NGC 6752 half-mass radius (CX 17), one point source $\sim 6'$ from the cluster center (the corresponding X-ray source falls on chip S4), and some diffuse X-ray emission centered on a bright extended radio source (possibly a head-tail radio galaxy) outside the cluster. At 1.4 GHz the radio counterpart to CX 17 has a flux density of 0.5 ± 0.1 mJy; no circular or linear polarization is detected from this source, with a 3 σ upper limit on the fractional polarization of 35%. At 2.4 GHz this source is marginally detected at the 3 σ level, with a flux density ~ 0.3 mJy.

The absolute astrometry of the ATCA data in the International Celestial Reference System (ICRS) is accurate to $\lesssim 0''.1$. Based on the two point-source coincidences, we corrected the *Chandra* astrometry to align these sources. The correction was $-0^s.044$ ($= -0''.33$) in right ascension and $-0''.17$ in declination.

4. OPTICAL OBSERVATIONS

The *HST* archive contains a substantial amount (~ 400 exposures) of WFPC2 imaging data covering the central regions of NGC 6752. Of particular utility are the data obtained by Bailyn and collaborators to suggest optical identification for two *ROSAT* sources in the core, the very ones we have now resolved into multiple *Chandra* sources. These consist of deep Hα_{656} (F656N filter; i.e., 6560 Å), R_{675} (F675W), and B_{439} (F439W) image sets, plus long time series in V_{555} (F555W) and I_{814} (F814W) covering the core alone

(for details, see Bailyn et al. 1996), ideal for the identification of Hα emission and/or variable stars. Furthermore, additional U_{336} (F336W) and nUV_{255} (F255W) are now available, allowing for additional UV excess selection. Unfortunately, not all of our *Chandra* sources have such complete optical coverage, owing to the nature of this archival data obtained for other unrelated projects. However, only one X-ray source (CX 8) lacks any *HST* color information at all.

In this section we will first outline the optical astrometry undertaken to tie the *HST* images to the ICRS and thereby facilitate the alignment of our *Chandra* detections. We will then proceed to describe our optical data preparation and reductions and end with our results.

4.1. *Optical Astrometry*

We aim to tie each *HST* pointing to the ICRS by finding matches between stars appearing on *HST* images and stars with accurate positions in either the Tycho 2 (Høg et al. 2000) or USNO-A2.0 (Monet 1998) catalogs. Unfortunately, owing to the brightness and stellar density of the cluster core, neither catalog extends to within 5′ of the center. However, the *HST* archive also contains numerous (largely *V*-band) images extending from the cluster center out to a ∼10′ radius, and these outermost images do overlap with the USNO-A2.0 coverage. On the basis of the *HST* pointing information (contained in each image header), we used the IRAF/STSDAS routine " metric " (which includes corrections for geometrical distortions toward the edge of each chip) to overplot the nominal USNO star positions. To aid in the matching, we also then degraded the *HST* images by convolving with a Gaussian to approximate the typical ground-based seeing of the plates used in deriving the catalog. It was then possible to make 58 reliable matches on two separate *HST* data sets (i.e., from different satellite pointings), deriving offsets of 1″.1 and 0″.1 in right ascension and declination, respectively. We found no evidence for a significant discrepancy in the nominal roll angle, and hence, we made no correction to this parameter. Taking the scatter to the astrometric fit and, in particular, the uncertainty in the roll angle, we estimate residual uncertainties of a few tenths of an arcsecond.

Having aligned these outermost *HST* images, we then had to step in via intermediate overlapping *HST* images to find corrections for all the useful images of the cluster center. The procedure was essentially the same for each step. We measured the centroids of all bright (but not saturated) stars appearing in the overlap regions of two *HST* data sets and then applied " invmetric " to derive their nominal right ascension and declination according to the headers. Pairs were then matched and average offsets in sky coordinates calculated. Again, in no case did there appear to be any significant roll angle discrepancies present. For these steps, we more typically found a few hundred matches, and hence, the uncertainty in the measured offsets was negligible relative to that of the initial tie to the USNO-A2.0 (ICRS) frame.

The final stage made use of the prior identifications of two Hα bright stars by Bailyn et al. (1996). Overplotting our *Chandra* sources for the core revealed that the two optical stars flagged in the Bailyn et al. finding chart (their Fig. 2) are indeed excellent matches to two of our X-ray sources. Specifically, our analyses of the relative positions and position angles in both the X-ray and the optical for

these two flagged stars were fully in agreement (Note that our astrometric solution for the position of these two objects differs in right ascension and declination by 0ˢ.33 [=2″.6] and 8″.4, respectively, from the positions given by Bailyn et al. 1996. We can suggest no explanation for this large discrepancy.) In our analysis, only a small ∼0″.5 X-ray versus optical offset remained. However, this is consistent with the expected uncertainty in our astrometric solution for these *HST* images relative to the ICRS frame. Hence, we decided to apply this small offset (assuming that these two stars are exactly at their *Chandra* positions) to the astrometry for all of our *HST* data sets. In order to be thorough, we opted to examine all optical/UV stars within ∼0″.5 of each *Chandra* source position. Indeed, as we describe in detail below, we then uncovered at least three more strong candidate optical counterparts, none of which were more than 0″.1 from the expected position based on this offset. Such results are indeed consistent with uncertainties expected in the relative astrometry of the X-ray positions combined with their transfer to a variety of *HST* data sets.

4.2. *Optical Data Reductions and Analysis*

The data from the *HST* archive are already well calibrated (aside from astrometry), and only two steps remained. For each pointing and filter, at least two images were available, which were then used to remove the numerous cosmic-ray events detected in each exposure. We used the " combine " task to calculate an average image and applied one-sided sigma clipping (based on the median value of each pixel and a noise model for the detector) to exclude cosmic-ray events. The images from each of the four chips were then trimmed to remove the partially masked edge regions.

We employed " daofind " in the IRAF implementation of DAOPHOT II (Stetson 1992) to find all stars detected at approximately 3 σ above background, and we then determined their centroids. Unfortunately, this method is not foolproof, and we also had to add a number of faint stars by hand to our list and delete others affected by the ∼20 saturated stars appearing on each frame. We excluded all stars with centers within ∼10–15 pixels of any saturated pixels and also any stars lying on the cross-shaped diffraction patterns of the very brightest stars. Having thus created a master star list for each image, aperture photometry yielded magnitudes for a range of annuli close to the measured FWHM of the PSF. We note that for the undersampled stellar PSFs of the Planetary Camera (PC) and especially the Wide Field (WF) chips, aperture photometry produced better results than our attempts at PSF fitting. The apertures we used are, however, far smaller than the standard 0″.5 aperture of the STMAG system (Holtzmann et al. 1995), and we therefore estimated the corresponding magnitude offsets needed relative to this large aperture for a number of bright (but nonsaturated) and isolated stars on both the PC and WF chips. Applying both these offsets and the appropriate zero points based on the sensitivity information in each header, we finally arrived at the STMAGs in a given filter for each star. We note that accurate estimation of the background contribution (especially critical for the faintest stars) is very difficult in such a crowded field. We adopted the mode value for an annulus surrounding each star. Tests, using either a fixed value as determined by averaging the results for the least crowded stars (farther from the core) or

TABLE 4
SUMMARY OF COLOR SELECTION FOR OPTICAL/UV COUNTERPARTS

| OPTICAL STAR ID | OFFSET FROM CXO POSITION[a] | | R_{675} | $H\alpha_{656}-R_{675}$ | $B_{439}-R_{675}$ | U_{336} | $U_{336}-V_{555}$ | $nUV_{255}-U_{336}$ |
	R.A. (arcsec)	Decl. (arcsec)						
1.............	0.05	0.05	19.36 ± 0.02	-0.24 ± 0.03	-0.96 ± 0.02	19.78 ± 0.06	0.24 ± 0.08	0.05 ± 0.15
							0.96 ± 0.06	
2.............	−0.09	0.07	19.55 ± 0.01	-0.86 ± 0.07	-0.23 ± 0.02	19.83 ± 0.06	0.40 ± 0.06	0.36 ± 0.17
3.............	0.06	−0.11	21.48 ± 0.03	-0.07 ± 0.08	-0.19 ± 0.05	21.8 ± 0.2[b]	0.2 ± 0.2[b]	...
4.............	−0.01	0.06	20.83 ± 0.05	-0.76 ± 0.07	0.25 ± 0.13	20.14 ± 0.08	-0.33 ± 0.13	-0.05 ± 0.19
							-0.75 ± 0.09	
5.............	−0.02	0.00	19.13 ± 0.01	-0.12 ± 0.03	0.03 ± 0.02	19.72 ± 0.06	0.73 ± 0.13	1.82 ± 0.19
							0.68 ± 0.24	
6.............	−0.09	0.00	23.63 ± 0.27	-0.34 ± 0.49	-0.96 ± 0.32	...	...	...
7.............	0.01	−0.06	21.44 ± 0.06	-1.40 ± 0.08	-0.10 ± 0.10	21.78 ± 0.21	0.08 ± 0.26	...
							0.48 ± 0.21	
10............	0.06	−0.05	...	...	...	19.67 ± 0.06		0.97 ± 0.19
							-0.27 ± 0.08	
11............	−0.05	0.05	21.60 ± 0.28	-0.41 ± 0.35	0.07 ± 0.39	...	...	...
13............	0.13	0.16	24.26 ± 0.15	-0.06 ± 0.47	-0.70 ± 0.20	...	...	...
15............	0.21	−0.18	...	...	...	22.16 ± 0.24	0.16 ± 0.25	-0.62 ± 0.54
16............	0.06	−0.18	19.05 ± 0.01	-0.17 ± 0.02	-0.05 ± 0.01	...	...	...

[a] The optical position is then given by *Chandra* X-ray value plus offset in each coordinate. Note that the results are in true seconds of arc for both right ascension and declination.

[b] These magnitudes are estimates based on the wide U (F300W) and wide V (F606W) data available ($U_{300} = 21.85 \pm 0.06$, $U_{300}-V_{606} = 0.36 \pm 0.06$) and transformations given in Holtzmann et al. 1995.

the centroid of a Gaussian fit to the "sky" histogram instead of the mode, showed that we can expect systematic errors of ~0.1–0.2 mag in our final STMAG values. We have also applied approximate corrections to the magnitudes derived from aperture photometry to compensate for the time-dependent charge transfer efficiency effect and the so-called long versus short anomaly, according to the formulae presented on the WFPC2 instrument Web pages.[14]

We constructed a variety of CMDs with all the available data. The most informative of these diagrams are shown in Figure 3, on which *all* stars located within the 0″.5 *Chandra* error circles are indicated by gray boxes. Numbers have been assigned to all candidate counterparts corresponding to the "CX" designation (i.e., our star 1 is the counterpart to CX 1). In this scheme, stars 1 and 2 of Bailyn et al. (1996) are CX 4 and CX 7, respectively. In some cases, candidates are only abnormal in certain colors, but they are all labeled in each diagram. The results on each star are summarized in Table 4 and § 5, and finding charts are shown in Figure 4.

5. RESULTS

The X-ray luminosities for the *Chandra* sources as listed in Tables 1 and 2 are in a range covered in the Galactic disk by CVs, RS CVn binaries, and MSPs (see, e.g., Fig. 8 in Verbunt et al. 1997). The soft X-ray transients with neutron stars in the Galactic disk tend to have higher luminosities (the lowest luminosity known to us is that of Cen X-4 measured in 1995 August with the *ROSAT* HRI at 7×10^{31} ergs s^{-1} between 0.5 and 2.5 keV; Rutledge et al. 2001b). Transients with a black hole have quiescent luminosities down to $\sim 10^{30}$ ergs s^{-1}; these luminosities may be due to chromospheric emission from the companion to the black hole,

however (Rutledge et al. 2000). None of the X-ray spectra in our sample are as soft as would be expected for a low-mass X-ray transient in quiescence; all systems with enough signal (CX 1–9), except CX 8, can be fitted with relatively hard thermal bremsstrahlung spectra, as expected for CVs.

A further clue to the nature of the *Chandra* sources may be obtained from the X-ray–to–optical flux ratio. For the *Chandra* sources whose optical counterparts have not been measured in V, we estimate $V \simeq 0.5(B + R)$. To allow comparison with the large database of *ROSAT*, we estimate that one X_{soft} *Chandra* count for our 29 ks NGC 6752 observation corresponds to a rate of 0.9×10^{-5} count s^{-1} in channels 52–201 of the *ROSAT* PSPC. As shown in Figure 5, the ratio of optical to X-ray flux of most *Chandra* sources in NGC 6752 suggests that they are cataclysmic variables. We discuss these first and the possible exceptions of CX 12, CX 16, and CX 18 later.

Figure 3 shows that the optical counterparts to CX 1, CX 2, CX 3, CX 4, CX 7, CX 10, and CX 15 all have ultraviolet excesses (at U_{336} and/or nUV_{255}) with respect to the main sequence, as expected for cataclysmic variables. In $B_{439}-R_{675}$, the optical counterparts to CX 1, CX 3, and CX 7 are still blue with respect to the main sequence, CX 2 and CX 4 are not distinguishable from the main sequence, no information is available on CX 10, and CX 15, CX 6, CX 11, and CX 13, for which no ultraviolet fluxes are available, are bluer than the main sequence in B_{439}. CX 1, CX 2, CX 4, and CX 7 also show clear Hα emission, and CX 3, CX 6, and CX 13 do not. CX 11 shows marginal Hα excess, and no information is available for CX 10 and CX 15. On the whole, the optical properties for all these objects are compatible with those expected for cataclysmic variables, although CX 11 and CX 15 show evidence for having spatially extended emission and could be background galaxies. These and other early *Chandra* observations are finding the
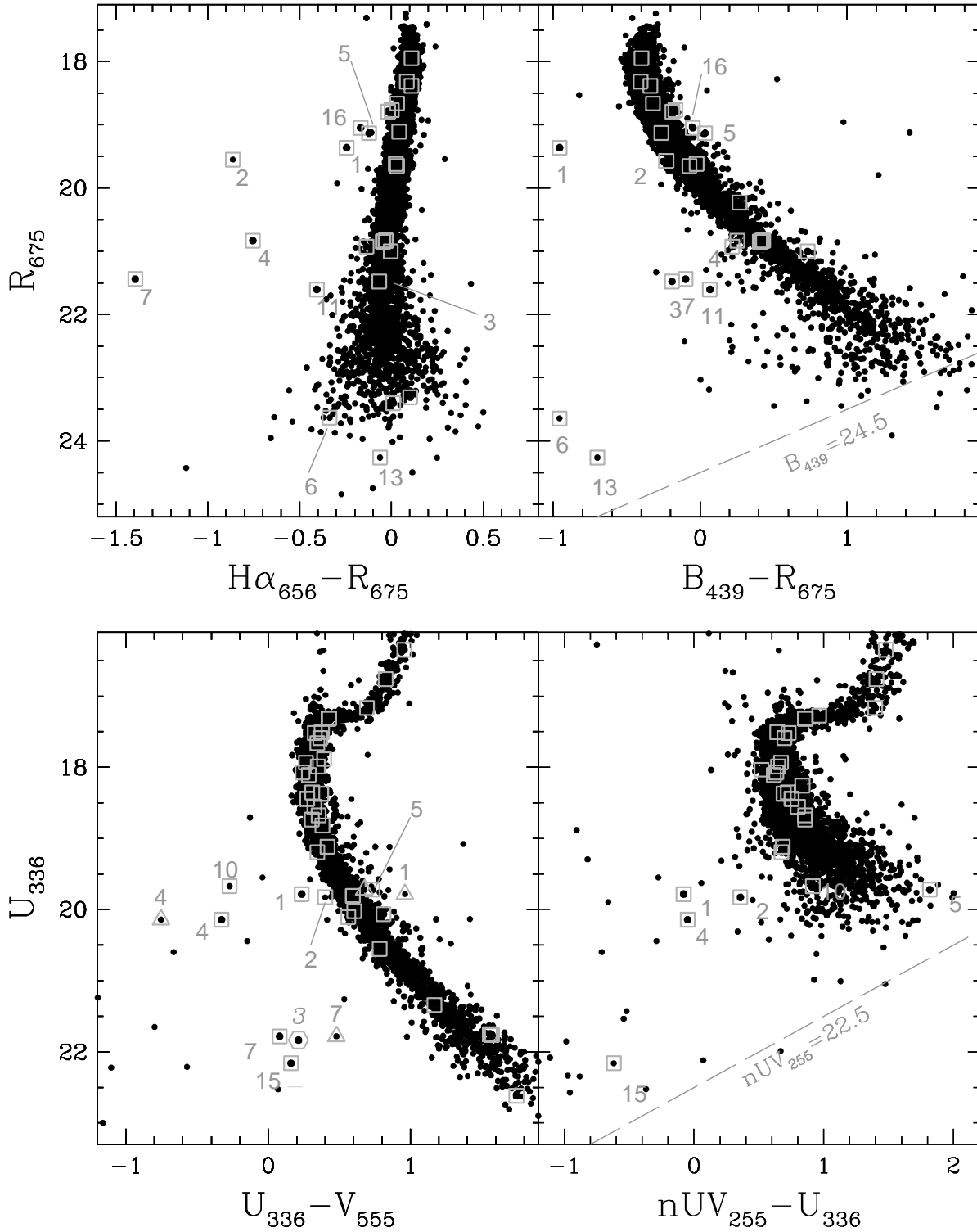
[14] See http://www.stsci.edu/instruments/wfpc2.

Fig. 3.—CMDs for the central regions of NGC 6752. All the stars from both the PC field and one of the WF chip fields are plotted along with all stars within 0″.5 of the *Chandra* source positions (indicated by gray boxes). The numbers refer to the candidate optical counterparts to the X-ray sources. All the R_{675}-, $H\alpha_{656}$-, and B_{439}-band data shown in the upper panels are taken from *HST* observations in 1994 August, whereas the U_{336}, V_{555}, and nUV$_{255}$ data in the lower panels were obtained in 2001 March. Note that in the bottom left-hand panel (1) four candidates are plotted twice, according to their colors calculated from V_{555} band either data taken contemporaneously (i.e., that of 2001 March, *squares*) or older data from 1994 August (*triangles*), which clearly show that three of them are variable; (2) the data for star 3 (*hexagon*) were obtained in the wide U (F300W) and wide V (F606W) filters and have been transformed before plotting.

long sought but, until recently, rarely observed population of CVs in globular clusters (Grindlay et al. 2001a, 2001b).

CX 12, CX 18, and CX 16 have (limits to) X-ray–to–optical flux ratios in the range of RS CVn systems. The

limited information that may be obtained from the X-ray hardness of these three sources indicates that they may be as soft as expected for RS CVn systems. Interestingly, the $B_{439}-R_{675}$ color of CX 16 places it on or slightly above the
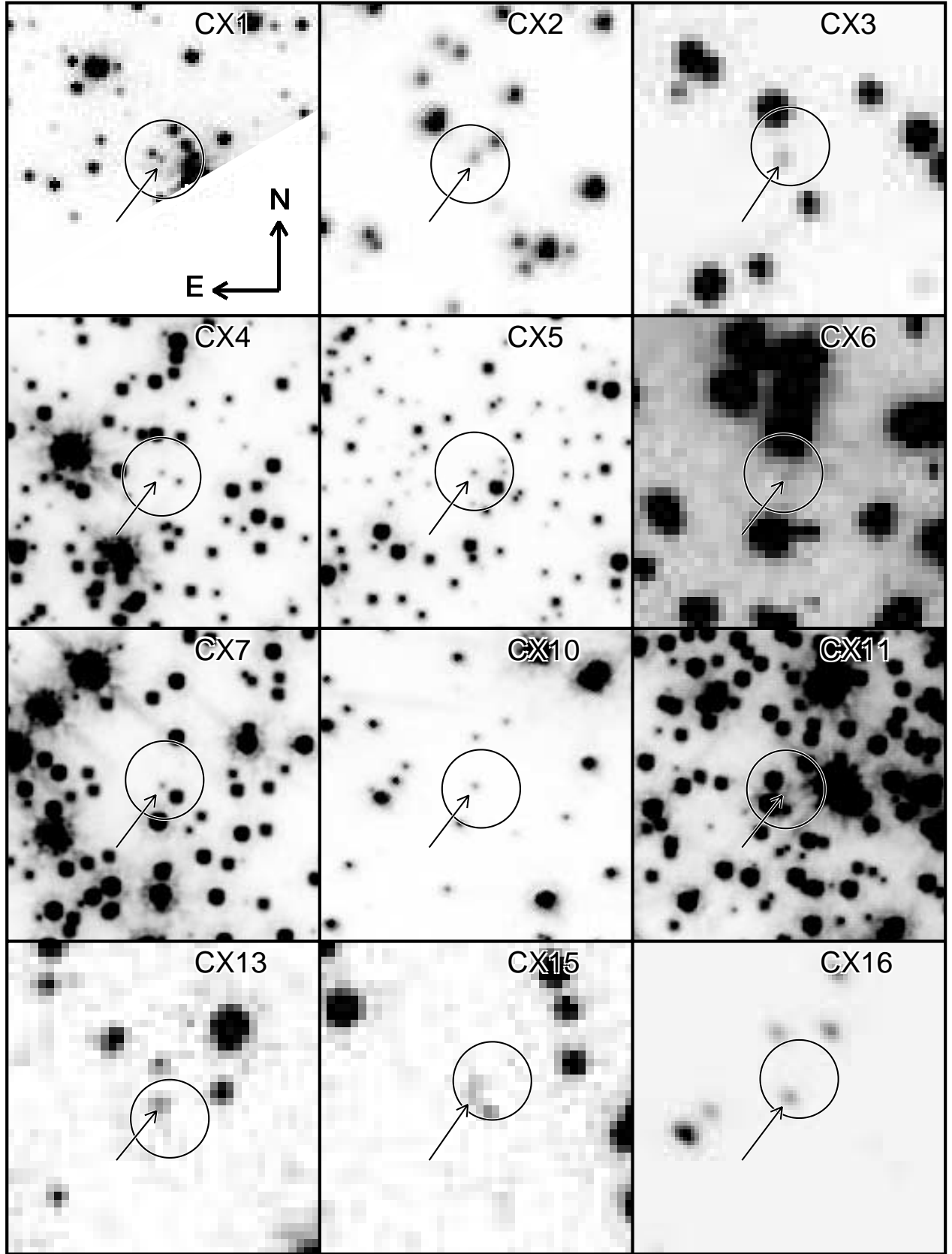
FIG. 4.—4″ × 4″ finding charts for each optical counterpart candidate, obtained from *HST* archival data. These images were taken in V_{555}, apart from the charts for stars 1 (U_{336}), 3, 6, 13 (B_{439}), and 14 (U_{336}), for which either V_{555} was unavailable or the counterpart too blue or crowded to be visible. We have overlaid the 0″5 radius error circles for the *Chandra* source positions (in which we searched), and the candidate stars themselves are indicated by arrows. We also note that the depth, gray scaling, and pixel scales for the images are varied since we have chosen the deepest, most well-sampled images (using dithered images where available) and then adjusted the gray scale to enhance visibility of the candidates.

Fig. 5.—Comparison of the X-ray and optical fluxes of *Chandra* sources (*numbers*) in NGC 6752 to those of field sources (C: Cen X-4; A: Aql X-1; T: X9/V1 and X19/V2 in 47 Tuc; see Verbunt & Hasinger 1998 for more details). *R* is the equivalent *ROSAT* count rate in channels 52–201. V_1 is the visual magnitude and for CVs is the magnitude at which the system is most commonly found. *Chandra* sources with only optical upper limits are indicated by arrows. The top dotted line roughly separates soft X-ray transients (above) from CVs (below). The bottom dotted line roughly separates CVs from RS CVn systems (below).

main sequence (see Fig. 3); its weak Hα emission is not unprecedented in RS CVn–type systems either. The optical counterparts for CX 12 and CX 18 would have visual fluxes more than about 3 mag fainter than our limits if they were dwarf novae in quiescence. They can be as bright as our limits if they are dwarf novae in outburst or nova-like variables of the UX UMa type (i.e., nonmagnetic, permanently bright CVs).

The location of CX 5 in the optical CMDs is similar to that of CX 16, as is its moderate Hα emission. This suggests that it is an RS CVn system (more precisely, a BY Dra system). Its high X-ray–to–optical flux ratio and spectral hardness are more suggestive of a cataclysmic variable, however.

As remarked above, our *Chandra* sources have X-ray luminosities in the range also observed for MSPs in the Galactic disk. In this respect, the X-ray sources for which we have no optical counterparts could be MSPs. Also, as stated in § 2.2, we expect approximately four serendipitous background sources within the half-mass radius. The optically unidentified faint X-ray sources may well be such background sources. Alas, no period derivatives or positions are as yet available for the five MSPs, with periods ranging from 3.3 to 9.0 ms, now known in NGC 6752 (Possenti et al. 2001b). The X-ray luminosity of an MSP is only a small fraction of the spin-down luminosity (Verbunt et al. 1996; Possenti et al. 2001a), and the latter is proportional to P^{-3} (with P the pulse period). To illustrate this, we write the X-ray luminosity L_X as a fraction f of the spin-

down luminosity $\dot{E}_{sd}$,

$$L_X = f\dot{E}_{sd} = \frac{4\pi^2 I f \dot{P}}{P^3} = \frac{2\pi^2 I f}{\tau_c P^2}, \quad (1)$$

where $I \simeq 10^{45}$ g cm^2 is the moment of inertia of the neutron star, $\tau_c \equiv P/(2\dot{P})$ its characteristic age, and $\dot{P}$ the intrinsic period derivative. Entering characteristic values, we obtain

$$L_X = 7 \times 10^{30} \text{ ergs s}^{-1} \frac{f}{0.001} \frac{10^{10} \text{ yr}}{\tau_c} \left(\frac{0.003 \text{ s}}{P}\right)^2. \quad (2)$$

We think that the most likely candidates are PSRs J1910−59A, C, and E, which have the shortest periods and should therefore be the brightest in X-rays. The least luminous X-ray sources appear the more likely candidates, in particular CX 17, which has a radio counterpart. However, CX 8 has a very soft spectrum and in our view cannot be excluded.

All of our likely source identifications are indicated in the X-ray CMD (Fig. 2).

6. DISCUSSION

Our *Chandra* observation provides a dramatic improvement over the *ROSAT* HRI observations. The central X-ray emission of NGC 6752, resolved into four sources by the *ROSAT* HRI, is now found to be due to 10 sources. The
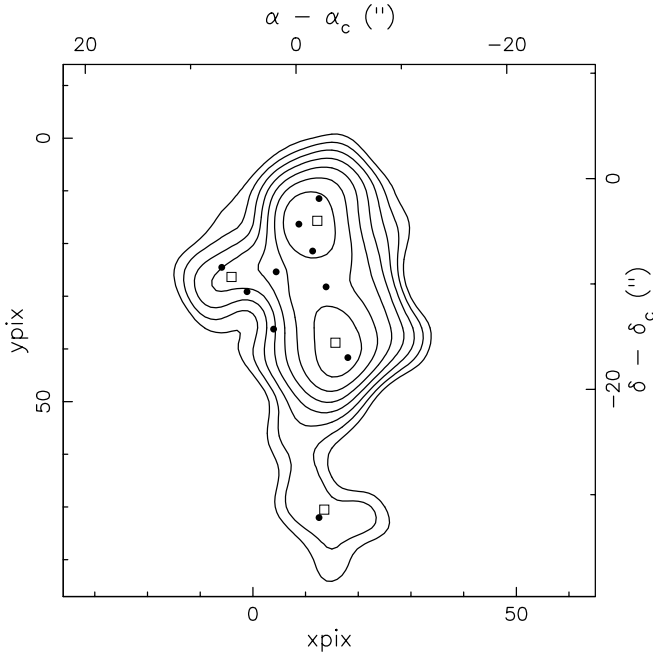
Fig. 6.—*ROSAT* HRI contours of NGC 6752 with positions of the central *Chandra* sources superposed (*filled circles*). *ROSAT* centroids are also indicated (*boxes*). The *ROSAT* contours were shifted (based on the correspondence of CX 2 and CX 3 with X14 and X6, respectively, from Verbunt & Johnston 2000) to align them with the *Chandra* frame.

very accurate positions of these and other newly discovered sources allow secure identifications with *HST* sources and with one radio source.

Outside the core, the two sources, CX 2 and CX 3, correspond to the *ROSAT* sources X14 and X6, respectively. From these two we determine an offset of $(1''9, -2''1)$, which has to be applied to the *ROSAT* positions (as given by Verbunt & Johnston 2000) to align them with the *Chandra* frame.

In Figure 6 we show the positions of the central sources that we have detected with *Chandra* superposed on a contour of the *ROSAT* HRI observation to which this offset has been applied. We then find that CX 6 and CX 1 correspond to X22 and X7b, respectively, whereas *ROSAT* source X7a has been resolved into CX 11, CX 12, and CX 14 and X21 into CX 4, CX 5, CX 7, and CX 9.

From our spectral fits to the *Chandra* sources, we can estimate the *ROSAT* HRI and PSPC count rates for the luminosities at which *Chandra* detected them: 1 X_{soft} *Chandra* count in our observation corresponds to about 0.0045 count

ks^{-1} in the *ROSAT* HRI observations and to 0.009 count ks^{-1} (channels 52–201) in the *ROSAT* PSPC observation. With this conversion we find that the luminosities of X14/CX 2, X6/CX 3, X22/CX 6, X7a/(CX 4, CX 5, CX 7, CX 9), and X21/(CX 11, CX 12, CX 14) are constant within the errors between the *ROSAT* HRI and *Chandra* observation. Source X7b/CX 1, however, was about 30% brighter in the *ROSAT* HRI than in the *Chandra* observation. The central conglomerate of sources was about 40% brighter during the *ROSAT* PSPC observation than during the *Chandra* observation; because of the lack of spatial resolution in the PSPC, we cannot assign this to a specific *Chandra* source. We thus have evidence that the X-ray luminosity of at least one central source, CX 1, is variable. Both X-ray and optical variability will be discussed in detail in L. Homer et al. (2002, in preparation).

Chandra observations have been published for three other globular clusters that do not contain a bright ($L_X > 10^{36}$ ergs s^{-1}) central X-ray source. The numbers of *identified* sources of various types are summarized in Table 5. Of these clusters, 47 Tuc has a larger core and slightly smaller central density than NGC 6752, causing the frequency of close encounters in 47 Tuc to be a factor of ~10 larger than that in NGC 6752. NGC 6397 has a higher core density and much smaller core radius than NGC 6752, leading to a frequency of close encounters a factor of ~10 smaller than in NGC 6752. Finally, ω Cen has a smaller central density and larger core than any of these clusters and an encounter frequency similar to that in NGC 6752.

The X-ray luminosity of currently known quiescent soft X-ray transients with neutron stars in the Galactic disk does not drop below ~10^{32} ergs s^{-1}. If a similar lower limit holds for such transients in globular clusters, the *Chandra* observations provide a complete census of the quiescent transients in the observed four clusters since none of the unclassified sources has an X-ray luminosity in excess of this threshold. If the number of quiescent soft X-ray transients scales with the collision frequency, we estimate that one such system is formed per ~30 of our normalized encounter frequencies, in which case the numbers of two, one, and zero in 47 Tuc, ω Cen, and NGC 6752 are well within expectation with Poisson statistics. The possible presence of such a source in NGC 6397, however, is somewhat surprising. A similar statement may be made for the X-ray–detected MSPs: for an expected number of one per 10 normalized encounter frequencies, only NGC 6397 is surprising in containing one. The presence of both a soft X-ray transient and an X-ray–detected MSP in NGC 6397 suggests that clusters with the highest densities contain more such systems than

TABLE 5
NATURE OF THE FAINT GLOBULAR CLUSTER X-RAY SOURCES

Cluster	Collision Frequency[a]	qLMXB	CV	Binaries[b]	MSP[c]	Unclassified	References
47 Tuc.........	≡100	2	13	5	9	~60	1
ω Cen	16	1	2	0	0	~20	2
NGC 6752...	9	0	11–14	1–3	1	6	3
NGC 6397...	1	1	8	2	1	1	4

[a] Collision frequency scaled on the frequency in 47 Tuc. It is computed based on the central density ρ_0 and core radius r_c given in the 1999 June 22 version of the catalogue, described in Harris 1996 as $\propto \rho_0^2 r_c^3$.

[b] X-ray–active main-sequence binaries.

[c] X-ray–detected MSPs.

REFERENCES.—(1) Grindlay et al. 2001a; (2) Rutledge et al. 2001a; (3) this paper; (4) Grindlay et al. 2001b.

indicated by the (average) collision number. This may be the consequence of more pronounced mass segregation in these clusters, which enhances the encounter rate of neutron stars with respect to the average encounter rate by concentrating them to the core.

The relative numbers of cataclysmic variables and binaries with a neutron star (i.e., permanently bright low-mass X-ray binaries or soft X-ray transients) according to theory depends on a number of factors including the retention fraction of neutron stars (many neutron stars may be born with velocities that throw them out of the cluster, whereas all white dwarfs remain), the mass segregation in the cluster (which will concentrate the remaining neutron stars to the core where the close encounters occur, more so than the less massive white dwarfs), and the importance of primordial binaries evolving into cataclysmic binaries (important in clusters with small encounter frequencies). It is therefore interesting to see that the number ratio of (hitherto classified) cataclysmic variables to soft X-ray transients is not significantly different in 47 Tuc and NGC 6397 even though their encounter frequencies differ by 2 orders of magnitude. If many of the unclassified sources in 47 Tuc turn out to be cataclysmic variables, as is expected, the number ratio of cataclysmic variables to soft X-ray transients in it will even be higher. This again suggests that the average collision number of NGC 6397 underestimates the neutron star encounter rate. It should be noted that the census of cataclysmic variables through X-rays is certainly not complete since many cataclysmic variables observed in the Galactic disk have X-ray luminosities below our threshold of 2×10^{30} ergs s^{-1} (see, e.g., Fig. 8 in Verbunt et al. 1997). If we accept that X9/V1 and X19/V2 in 47 Tuc and CX 6 in NGC 6752 are indeed cataclysmic variables, we see from Figure 5 that their X-ray–to–optical flux ratio is higher than that of any cataclysmic variable in the Galactic disk studied by Verbunt et al. (1996). The high X-ray luminosity of X9 has been confirmed with *Chandra* observations; the relative hardness of its X-ray spectrum suggests a cataclysmic variable rather than a quiescent soft X-ray transient (Grindlay et al. 2001a)

Equally remarkable is the fact that the number ratios of cataclysmic variables to X-ray active binaries is approxi-mately 4 in all four clusters under discussion, notwithstanding the large range of encounter frequencies. In dense clusters like 47 Tuc, most cataclysmic variables should be formed via close encounters, whereas a less concentrated cluster like ω Cen may have a significant contribution of primordial binaries evolved into cataclysmic variables (Verbunt & Meylan 1988; di Stefano & Rappaport 1994; Davies 1997). As more sources are identified in 47 Tuc and ω Cen and other clusters are studied as well, the numbers may become big enough to allow more definite conclusions.

Finally, we are struck by the fact that all X-ray sources in Figure 1 lie in a quadrant south of the cluster center. The formal probability of this happening with 13 sources is small, but if the optical cluster center position is accurate, we are inclined to ascribe this to chance. At the small interstellar absorption toward NGC 6752 and with the relatively hard spectra of the X-ray sources, differential absorption over the cluster cannot explain the asymmetry. The optical cluster center would have to be in error by about $10''$ for it to be close to the X-ray center. We note that if this is the case, then NGC 6752 becomes the second globular cluster for which the optical determination of its center has been corrected by an X-ray observation (the first one being NGC 6541; see Fig. 1 of Verbunt 2001).

REFERENCES

Arnaud, K. A. 1996, in ASP Conf. Ser. 101, Astronomical Data Analysis Software and Systems V, ed. G. Jacoby & J. Barnes (San Francisco: ASP), 17
Asai, K., Dotani, T., Hoshi, R., Tanaka, Y., Robinson, C. R., & Terada, K. 1998, PASJ, 50, 611
Asai, K., Dotani, T., Mitsuda, K., Hoshi, R., Vaughn, B., Tanaka, Y., & Inoue, H. 1996, PASJ, 48, 257
Bailyn, C. D., Rubenstein, E. P., Slavin, S. D., Cohn, H., Lugger, P., Cool, A. M., & Grindlay, J. E. 1996, ApJ, 473, L31
Becker, W., & Trümper, J. 1999, A&A, 341, 803
Camilo, F., Lorimer, D. R., Freire, P., Lyne, A. G., & Manchester, R. N. 2000, ApJ, 535, 975
Davies, M. B. 1997, MNRAS, 288, 117
Davies, M. B., & Hansen, B. M. S. 1998, MNRAS, 301, 15
Deutsch, E. W., Anderson, S. F., Margon, B., & Downes, R. A. 1998, ApJ, 493, 775
di Stefano, R., & Rappaport, S. 1994, ApJ, 423, 274
Frater, R. H., Brooks, J. W., & Whiteoak, J. B. 1992, J. Electrical Electron. Eng. Australia, 12, 103
Freire, P. C., Camilo, F., Lorimer, D. R., Lyne, A. G., Manchester, R. N., & D'Amico, N. 2001, MNRAS, 326, 901
Geffert, M. 1998, A&A, 340, 305
Giacconi, R., et al. 2001, ApJ, 551, 624
Grindlay, J. E. 1993, in ASP Conf. Ser. 50, Structure and Dynamics of Globular Clusters, ed. S. Djorgovski & G. Meylan (San Francisco: ASP), 285

Grindlay, J. E., Heinke, C., Edmonds, P. D., & Murray, S. S. 2001a, Science, 292, 2290
Grindlay, J. E., Heinke, C. O., Edmonds, P. D., Murray, S. S., & Cool, A. M. 2001b, ApJ, 563, L53
Hakala, P. J., Charles, P. A., Johnston, H. M., & Verbunt, F. 1997, MNRAS, 285, 693
Harris, W. E. 1996, AJ, 112, 1487
Heinke, C. O., Edmonds, P. D., & Grindlay, J. E. 2001, ApJ, 562, 363
Hertz, P., & Grindlay, J. E. 1983a, ApJ, 267, L83
———. 1983b, ApJ, 275, 105
Høg, E., et al. 2000, A&A, 355, L27
Holtzmann, J. A., Burrows, C. J., Casertano, S., Hester, J. J., Trauger, J. T., Watson, A. M., & Worthey, G. 1995, PASP, 107, 1065
Homer, L., Anderson, S. F., Margon, B., Deutsch, E. W., & Downes, R. A. 2001, ApJ, 550, L155
Hut, P., et al. 1992, PASP, 104, 981
in 't Zand, J. J. M., et al. 1999, A&A, 345, 100
Johnston, H. M., Verbunt, F., & Hasinger, G. 1994, A&A, 289, 763
Lewin, W. H. G., van Paradijs, J., & Taam, R. E. 1993, Space Sci. Rev., 62, 223
Lyne, A. G., Brinklow, A., Middleditch, J., Kulkarni, S. R., & Backer, D. C. 1987, Nature, 328, 399
Margon, B., Downes, R. A., & Gunn, J. E. 1981, ApJ, 247, L89
Monet, D. G. 1998, BAAS, 193, 120.03
Pooley, D., Lewin, W. H. G., Verbunt, F., Fox, D. W., Margon, B., Kaspi, V. M., van der Klis, M., & Miller, J. M. 2000, BAAS, 32, 29.01

Possenti, A., Cerutti, R., Colpi, M., & Mereghetti, S. 2001a, A&A, submitted (astro-ph/0109452)
Possenti, A., D'Amico, N., Manchester, R. N., Sarkissian, J., Lyne, A. G., & Camilo, F. 2001b, A&A, submitted (astro-ph/0108343)
Predehl, P., & Schmitt, J. H. M. M. 1995, A&A, 293, 889
Renzini, A., et al. 1996, ApJ, 465, L23
Richman, H. R. 1996, ApJ, 462, 404
Rutledge, R. E., Bildsten, L., Brown, E. F., Pavlov, G. G., & Zavlin, V. E. 2000, ApJ, 529, 985
———. 2001a, ApJ, submitted (astro-ph/0105405)
———. 2001b, ApJ, 551, 921
Saito, Y., Kawai, N., Kamae, T., Shibata, S., Dotani, T., & Kulkarni, S. R. 1997, ApJ, 477, L37
Stetson, P. B. 1992, in ASP Conf. Ser. 25, Astronomical Data Analysis Software and Systems I, ed. D. W. Worrall, C. Biemesderfer, & J. Barnes (San Francisco: ASP), 297

Trager, S. C., Djorgovski, S., & King, I. R. 1993, in ASP Conf. Ser. 50, Structure and Dynamics of Globuler Clusters, ed. S. Djorgovski & G. Meylan (San Francisco: ASP), 347
van Teeseling, A., Beuermann, K., & Verbunt, F. 1996, A&A, 315, 467
Verbunt, F. 2001, A&A, 368, 137
Verbunt, F., Belloni, T., Johnston, H. M., van der Klis, M., & Lewin, W. H. G. 1994, A&A, 285, 903
Verbunt, F., Bunk, W. H., Ritter, H., & Pfeffermann, E. 1997, A&A, 327, 602
Verbunt, F., & Hasinger, G. 1998, A&A, 336, 895
Verbunt, F., & Johnston, H. M. 2000, A&A, 358, 910
Verbunt, F., Kuiper, L., Belloni, T., Johnston, H. M., de Bruyn, A. G., Hermsen, W., & van der Klis, M. 1996, A&A, 311, L9
Verbunt, F., & Meylan, G. 1988, A&A, 203, 297
Weisskopf, M. C., O'Dell, S. L., & van Speybroeck, L. F. 1996, Proc. SPIE, 2805, 2